PHYSICAL REVIEW D **89,** 074015 (2014)

Chiral perturbation theory and the $\bar{B}\bar{B}$ strong interaction

Zhan-Wei Liu,[*] Ning Li,[†] and Shi-Lin Zhu[‡]

Department of Physics and State Key Laboratory of Nuclear Physics and Technology Peking University, Beijing 100871, China

(Received 16 December 2012; revised manuscript received 6 February 2014; published 4 April 2014)

We have calculated the potentials of the heavy (charmed or bottomed) pseudoscalar mesons up to $O(\epsilon^2)$ with the heavy meson chiral perturbation theory. We take into account the contributions from the football, triangle, box, and crossed diagrams with the 2ϕ exchange and one-loop corrections to the contact terms. We notice that the total 2ϕ-exchange potential alone is attractive in the small momentum region in the channel $\bar{B}\bar{B}^{I=1}$, $\bar{B}_s\bar{B}_s{}^{I=0}$, or $\bar{B}\bar{B}_s{}^{I=1/2}$, while repulsive in the channel $\bar{B}\bar{B}^{I=0}$. Hopefully the analytical chiral structures of the potentials may be useful in the extrapolation of the heavy meson interaction from lattice QCD simulation.

DOI: 10.1103/PhysRevD.89.074015 PACS numbers: 12.39.Fe, 14.40.Lb, 14.40.Nd, 34.20.Gj

I. INTRODUCTION

Since the discovery of $X(3872)$ [1], many charmoniumlike and bottomoniumlike states such as $X(3940)$ [2] and $X(4160)$ [3] have been observed in the past decade. The charmoniumlike state $X(3872)$ was first observed by the Belle Collaboration in the exclusive decay process $B^{\pm} \to K^{\pm}\pi^{+}\pi^{-}J/\psi$. Last year the Belle Collaboration observed two charged bottomoniumlike resonances $Z_b(10610)$ and $Z_b(10650)$ in the hidden-bottom decay channels $\pi^{\pm}\Upsilon(nS)$ $(n = 1, 2, 3)$ and $\pi^{\pm}h_b(mP)$ $(m = 1, 2)$ of $\Upsilon(5S)$ [4].

Some of these new states including the above two charged Z_b states do not fit into the conventional quark model framework. Various theoretical approaches including the lattice QCD [5], the QCD sum rule [6], and the quark model [7] have been employed to interpret the underlying structure of these new states. Despite huge experimental and theoretical efforts, the nature of some of these exotic states is still elusive.

For example, the interpretation of $X(3872)$ remains challenging since the discovery in 2003. One popular speculation is that $X(3872)$ is a molecular state composed of a pair of heavy mesons [8–10]. Similarly, the two charged $Z_b(10610)$ and $Z_b(10650)$ states are proposed as the $B\bar{B}^*$ and $B^*\bar{B}^*$ molecule states within the one boson exchange (OBE) framework [11,12].

Besides the charmoniumlike and bottomoniumlike states, the possible existence of some molecular candidates composed of $\bar{B}\bar{B}$ mesons and DD mesons is also very interesting. If the attractive interaction is strong enough between the heavy meson pair, this kind of states may exist. Their behavior will be very similar to the deuteron, which is composed of two nucleons. There have been some investigation of these interesting states within the OBE model.

However, the interaction potential derived from the OBE model contains several phenomenological coupling constants and cutoff parameters, which should in principle be extracted through fitting to the experimental data. Unfortunately, there is not much experimental information on the strong interaction between the light meson and heavy meson. It will be very desirable to derive the strong interaction between the heavy meson pair with a model-independent approach. Especially many new states such as $X(3872)$ and the two Z_b states lie very close to the threshold. Within these very loosely bound systems, the long-range pion exchange force should play an important role. Therefore the chiral perturbation theory provides a natural framework to investigate the heavy meson strong interaction. In this work, we shall derive the heavy pseudoscalar meson potential order by order.

Chiral perturbation theory (χPT) is a model-independent tool to study the chiral dynamics of heavy hadrons. Heavy hadron χPT is frequently used for the system made up with a single heavy hadron and light pseudoscalar mesons because of its explicit power counting [13–17]. The scattering matrix can be expanded order by order in the small parameter $\epsilon = p/\Lambda_\chi$, where p represents either the momentum of the light pseudoscalar mesons or the residual momentum of the heavy hadrons in the nonrelativistic limit, while Λ_χ represents either the scale of chiral symmetry breaking or the mass of heavy hadrons. The power counting guarantees that one can just calculate some limited Feynman diagrams and obtain the scattering matrix at the certain order.

Weinberg developed a new formalism and first extended the chiral perturbation theory to the two nucleon system [18,19]. Since his pioneering work, the modern nuclear force has been built upon the chiral effective field theory [20–30]. Such a formalism was used extensively to

[*]liuzhanwei@pku.edu.cn
[†]leening@pku.edu.cn
[‡]zhusl@pku.edu.cn

investigate the various few-nucleon observables such as the partial-wave analysis, few-nucleon scattering, and reaction.

As pointed out by Weinberg [18,19], the power counting of the two nucleon scattering matrix is broken by the double poles of the heavy hadrons in some two-particle-reducible (2PR) Feynman diagrams. Let us illustrate this point with the box diagram in Fig. 1. The Feynman amplitude can be written as

$$\begin{aligned} & i\int d^4l \frac{i}{l^0+P^0+i\varepsilon}\frac{i}{-l^0+P^0+i\varepsilon}\times\cdots \\ & \quad = i\int dl^0 \frac{i}{l^0+P^0+i\varepsilon}\frac{i}{-l^0+P^0+i\varepsilon}\int d^3l\cdots, \end{aligned} \quad (1)$$

where we omit the parts relevant to the pion that preserves the power counting. We will focus the integral with l^0 and work it out by closing the l^0 contour integral in the lower half-plane

$$\begin{aligned} \mathcal{I} &\equiv i\int dl^0 \frac{i}{l^0+P^0+i\varepsilon}\frac{i}{-l^0+P^0+i\varepsilon} \\ &= \frac{\pi}{P^0+i\varepsilon}\approx\frac{\pi}{\vec{P}^2/(2m_N)+i\varepsilon}. \end{aligned} \quad (2)$$

The naive power counting predicts that $\mathcal{I}$ should be $O(1/|\vec{P}|)$. But it is $O(m_N/|\vec{P}|^2)$ from Eq. (2). $\mathcal{I}$ is actually enhanced by a large factor $m_N/|\vec{P}|$ compared to the naive power counting prediction.

With Weinberg's formalism, we do not directly calculate the scattering matrix of the few hadrons perturbatively with the heavy hadron χPT due to the 2PR diagrams. Instead, we focus on the potential. In the derivation of the hadron-hadron potential, one takes into account the two-particle-irreducible (2PI) parts of the Feynman diagrams only and calculate the potential of the few hadrons perturbatively with the correct power counting. Afterwards, one can obtain the scattering matrix with the potential by solving the nonperturbative equations such as Schrödinger equations, Lippmann-Schwinger equations, and so on. The 2PR contributions will be recovered when solving the nonperturbative equations.

The reliable hadron-hadron potential is a necessary input for getting the scattering amplitude or phase shift of the hadrons. It is also essential to explore the existence of the heavy hadron molecules. For example, the binding energy or size of the molecular states can be obtained from the potentials of the hadrons by solving the Schrödinger or Lippmann-Schwinger equations.

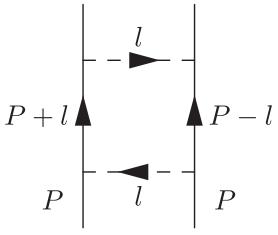

FIG. 1. The box diagram. The solid line represents the nucleon, and the dashed line represents the pion.

In this work, we shall use Weinberg's formalism to derive the $\bar{B}\,\bar{B}$ potentials in four independent channels up to the 1-loop level with heavy meson chiral perturbation theory (HMχPT). We include the heavy vector $\bar{B}^*$ mesons as explicit degrees besides the $\bar{B}$ and light pseudoscalar ϕ mesons since the $\bar{B}$ and $\bar{B}^*$ mesons would form a degenerate doublet in the limit of heavy quark symmetry. We count the mass difference Δ between $\bar{B}$ and $\bar{B}^*$ mesons as $O(\epsilon^1)$. The potentials of the $\bar{B}\,\bar{B}$ mesons start at $O(\epsilon^0)$. We will investigate the corrections up to $O(\epsilon^2)$.

This paper is organized as follows. In Sec. II, we list the Lagrangians of HMχPT. In Sec. III, we present the expressions of the $\bar{B}\,\bar{B}$ potential, which include the tree-level diagram contributions at the leading order and the loop corrections at $O(\epsilon^2)$. In Sec. IV, we give the numerical results of the $\bar{B}\,\bar{B}$ potentials in the first subsection. Then we present the results of the potentials of the DD mesons in the second subsection. We compare the results within different schemes in Sec. V. Section VI is a short summary.

II. LAGRANGIANS WITH HMχPT

The leading order $\bar{B}\,\bar{B}$ potential is at $O(\epsilon^0)$ and receives only the contribution from the tree-level diagrams made up of the vertices of the leading order Lagrangians in Eq. (3). The corrections start at $O(\epsilon^2)$. They contain the contributions of the 1-loop diagrams generated by the leading Lagrangians and the contributions of tree diagrams generated by the Lagrangians at higher order.

The leading Lagrangians are

$$\begin{aligned} \mathcal{L}^{(0)}_{4H} &= D_a \mathrm{Tr}[H\gamma_\mu\bar{H}]\mathrm{Tr}[H\gamma^\mu\bar{H}] \\ &\quad + D_b \mathrm{Tr}[H\gamma_\mu\gamma_5\bar{H}]\mathrm{Tr}[H\gamma^\mu\gamma_5\bar{H}] \\ &\quad + E_a \mathrm{Tr}[H\gamma_\mu\lambda^a\bar{H}]\mathrm{Tr}[H\gamma^\mu\lambda_a\bar{H}] \\ &\quad + E_b \mathrm{Tr}[H\gamma_\mu\gamma_5\lambda^a\bar{H}]\mathrm{Tr}[H\gamma^\mu\gamma_5\lambda_a\bar{H}], \end{aligned} \quad (3)$$

$$\begin{aligned} \mathcal{L}^{(1)}_{H\phi} &= -\langle (iv\cdot\partial H)\bar{H}\rangle + \langle Hv\cdot\Gamma\bar{H}\rangle + g\langle H\not{u}\gamma_5\bar{H}\rangle \\ &\quad -\frac{1}{8}\Delta\langle H\sigma^{\mu\nu}\bar{H}\sigma_{\mu\nu}\rangle, \end{aligned} \quad (4)$$

where the number in the parentheses represents the chiral dimension, $v_\mu=(1,\vec{0})$ is the velocity of a slowly moving heavy meson, and H represents the $\bar{B}$ and $\bar{B}^*$ doublet in the heavy quark symmetry limit,

$$\begin{aligned} H &= \frac{1+\not{v}}{2}(P^*_\mu\gamma^\mu + iP\gamma_5), \\ \bar{H} &= \gamma^0 H^\dagger\gamma^0 = (P^{*\dagger}_\mu\gamma^\mu + iP^\dagger\gamma_5)\frac{1+\not{v}}{2}, \end{aligned} \quad (5)$$

$$P = (B^-, \bar{B}^0, \bar{B}_s^0), \qquad P_\mu^* = (B^{*-}, \bar{B}^{*0}, \bar{B}_s^{*0})_\mu. \quad (6)$$

The pseudoscalar meson field, chiral connection, and axial vector field are defined as follows:

$$\Gamma_\mu = \frac{i}{2}[\xi^\dagger, \partial_\mu \xi], \qquad u_\mu = \frac{i}{2}\{\xi^\dagger, \partial_\mu \xi\}, \qquad \xi = \exp(i\phi/2f), \quad (7)$$

$$\phi = \sqrt{2}\begin{pmatrix} \frac{\pi^0}{\sqrt{2}} + \frac{\eta}{\sqrt{6}} & \pi^+ & K^+ \\ \pi^- & -\frac{\pi^0}{\sqrt{2}} + \frac{\eta}{\sqrt{6}} & K^0 \\ K^- & \bar{K}^0 & -\frac{2}{\sqrt{6}}\eta \end{pmatrix}. \quad (8)$$

The Lagrangian $\mathcal{L}_{4H}^{(0)}$ generates the contact interaction terms of the four bottomed mesons while $\mathcal{L}_{H\phi}^{(1)}$ depicts the interaction between the heavy mesons and light pseudoscalar mesons. The other contact terms with different Lorentz structures at the leading order are not independent. Actually they are linear combinations of terms in $\mathcal{L}_{4H}^{(0)}$, so we do not need them. For example, the term $\mathrm{Tr}[H\gamma_\mu \bar{H} H\gamma^\mu \bar{H}]$ can be expressed as the linear combination of terms in $\mathcal{L}_{4H}^{(0)}$ by the Fierz transformation. In the heavy meson limit, $\mathrm{Tr}[H\bar{H}]\mathrm{Tr}[H\bar{H}]$ and $\mathrm{Tr}[H\sigma_{\mu\nu}\bar{H}]\mathrm{Tr}[H\sigma^{\mu\nu}\bar{H}]$ can be absorbed by readjusting the coefficients D_a and D_b of $\mathcal{L}_{4H}^{(0)}$, respectively. The term $\mathrm{Tr}[H\gamma_5\bar{H}]\mathrm{Tr}[H\gamma^5\bar{H}]$ vanishes in the heavy meson limit. Similar conclusions hold for the terms containing λ^a such as $\mathrm{Tr}[H\gamma_5\lambda^a\bar{H}]\mathrm{Tr}[H\gamma^5\lambda_a\bar{H}]$.

The ranges of the couplings D_a, D_b, E_a, and E_b were estimated in the $D\bar{D}$ case by fixing the masses of $X(3872)$, $X(3915)$, and $Y(4140)$ and the isospin breaking branching ratio of $X(3872)$ in Ref. [31]. Their values lie from several to tens of GeV^{-2} with positive signs.

The $O(\epsilon^2)$ Lagrangian $\mathcal{L}_{4H}^{(2)}$ will also contribute to the potentials, which read

$$\begin{aligned}\mathcal{L}_{4H}^{(2,h)} &= D_a^h \mathrm{Tr}[H\gamma_\mu\bar{H}]\mathrm{Tr}[H\gamma^\mu\bar{H}]\mathrm{Tr}(\chi_+) + D_b^h \mathrm{Tr}[H\gamma_\mu\gamma_5\bar{H}]\mathrm{Tr}[H\gamma^\mu\gamma_5\bar{H}]\mathrm{Tr}(\chi_+) \\ &\quad + E_a^h \mathrm{Tr}[H\gamma_\mu\lambda^a\bar{H}]\mathrm{Tr}[H\gamma^\mu\lambda_a\bar{H}]\mathrm{Tr}(\chi_+) + E_b^h \mathrm{Tr}[H\gamma_\mu\gamma_5\lambda^a\bar{H}]\mathrm{Tr}[H\gamma^\mu\gamma_5\lambda_a\bar{H}]\mathrm{Tr}(\chi_+), \end{aligned} \quad (9)$$

$$\begin{aligned}\mathcal{L}_{4H}^{(2,d)} &= D_a^d \mathrm{Tr}[H\gamma_\mu\tilde{\chi}_+\bar{H}]\mathrm{Tr}[H\gamma^\mu\bar{H}] + D_b^d \mathrm{Tr}[H\gamma_\mu\gamma_5\tilde{\chi}_+\bar{H}]\mathrm{Tr}[H\gamma^\mu\gamma_5\bar{H}] \\ &\quad + E_a^d d^{abc}\mathrm{Tr}[H\gamma_\mu\lambda_a\bar{H}]\mathrm{Tr}[H\gamma^\mu\lambda_b\bar{H}]\mathrm{Tr}[\tilde{\chi}_+\lambda_c] + E_b^d d^{abc}\mathrm{Tr}[H\gamma_\mu\gamma_5\lambda_a\bar{H}]\mathrm{Tr}[H\gamma^\mu\gamma_5\lambda_b\bar{H}]\mathrm{Tr}[\tilde{\chi}_+\lambda_c], \end{aligned} \quad (10)$$

$$\begin{aligned}\mathcal{L}_{4H}^{(2,v)} &= \{D_{a1}^v \mathrm{Tr}[(v\cdot DH)\gamma_\mu(v\cdot D\bar{H})]\mathrm{Tr}[H\gamma^\mu\bar{H}] + D_{a2}^v \mathrm{Tr}[(v\cdot DH)\gamma_\mu\bar{H}]\mathrm{Tr}[(v\cdot DH)\gamma^\mu\bar{H}] \\ &\quad + D_{a3}^v \mathrm{Tr}[(v\cdot DH)\gamma_\mu\bar{H}]\mathrm{Tr}[H\gamma^\mu(v\cdot D\bar{H})] + D_{a4}^v \mathrm{Tr}[((v\cdot D)^2 H)\gamma_\mu\bar{H}]\mathrm{Tr}[H\gamma^\mu\bar{H}] \\ &\quad + D_{b1}^v \mathrm{Tr}[(v\cdot DH)\gamma_\mu\gamma_5(v\cdot D\bar{H})]\mathrm{Tr}[H\gamma^\mu\gamma_5\bar{H}] + \cdots + E_{a1}^v \mathrm{Tr}[(v\cdot DH)\gamma_\mu\lambda^a(v\cdot D\bar{H})]\mathrm{Tr}[H\gamma^\mu\lambda_a\bar{H}] + \cdots \\ &\quad + E_{b1}^v \mathrm{Tr}[(v\cdot DH)\gamma_\mu\gamma_5\lambda^a(v\cdot D\bar{H})]\mathrm{Tr}[H\gamma^\mu\gamma_5\lambda_a\bar{H}] + \cdots\} + \mathrm{H.c.}, \end{aligned} \quad (11)$$

$$\begin{aligned}\mathcal{L}_{4H}^{(2,q)} &= \{D_1^q \mathrm{Tr}[(D^\mu H)\gamma_\mu\gamma_5(D^\nu\bar{H})]\mathrm{Tr}[H\gamma_\nu\gamma_5\bar{H}] + D_2^q \mathrm{Tr}[(D^\mu H)\gamma_\mu\gamma_5\bar{H}]\mathrm{Tr}[(D^\nu H)\gamma_\nu\gamma_5\bar{H}] \\ &\quad + D_3^q \mathrm{Tr}[(D^\mu H)\gamma_\mu\gamma_5\bar{H}]\mathrm{Tr}[H\gamma_\nu\gamma_5(D^\nu\bar{H})] + D_4^q \mathrm{Tr}[(D^\mu D^\nu H)\gamma_\mu\gamma_5\bar{H}]\mathrm{Tr}[H\gamma_\nu\gamma_5\bar{H}] \\ &\quad + E_1^q \mathrm{Tr}[(D^\mu H)\gamma_\mu\gamma_5\lambda^a(D^\nu\bar{H})]\mathrm{Tr}[H\gamma_\nu\gamma_5\lambda_a\bar{H}] + \cdots\} + \mathrm{H.c.}, \cdots \end{aligned} \quad (12)$$

where d^{abc} is the totally symmetric structure constant of the SU(3) group, and

$$\tilde{\chi}_\pm = \chi_\pm - \frac{1}{3}\mathrm{Tr}[\chi_\pm], \qquad \chi_\pm = \xi^\dagger\chi\xi^\dagger \pm \xi\chi\xi,$$
$$\chi = \mathrm{diag}(m_\pi^2, m_\pi^2, 2m_K^2 - m_\pi^2). \quad (13)$$

The low-energy constants (LECs) in Eqs. (9)–(12) contain both the infinite and the finite parts. We will use the infinite parts to cancel the divergence introduced by the loop diagrams. We are unable to determine the finite parts of the LECs due to the lack of experimental data right now, which we tend to neglect for the moment. However, these LECs at $O(\epsilon^2)$ should be included in a complete analysis in the future when more experimental data are available.

There will be devoted efforts to study the new resonances composed of a pair of $\bar{B}^{(*)}B^{(*)}$ at the approved SuperBelle, KEK. The investigation of these systems may reveal the interaction between $\bar{B}^{(*)}B^{(*)}$. For example, one may know whether the interaction is attractive at some distance.

Moreover, right now there exists dedicated huge efforts to study the $\bar{D}^{(*)}D^{(*)}$ interaction through the decays of the excited charmonium resonances at BESIII/BEPCII at IHEP, Beijing. In quantum field theory, the $\bar{B}^{(*)}B^{(*)}$ interaction could be related to the $\bar{B}^{(*)}\bar{B}^{(*)}$ except the short distance part due to the annihilation in the $\bar{B}^{(*)}B^{(*)}$ channel [32,33].

Besides, using lattice QCD within the Lüscher's formalism, the scattering length and the scattering phase shifts have been studied for pion-pion scattering, $D^*\bar{D}_1$ scattering, and so on [34–36]. If there were lattice studies about the $\bar{B}\bar{B}$ or DD scattering in different partial waves and different channels, we could fix some parameters or reduce the number of independent parameters with the lattice information. In Appendix B we fit some LECs with the results of quenched lattice QCD. In our subsequent work, we also plan to reduce the number of independent LECs by assuming large N_c and heavy quark symmetry as used in Ref. [37].

$\mathcal{L}_{4H}^{(2,h)}$ and $\mathcal{L}_{4H}^{(2,d)}$ are made up of four heavy meson fields, $\mathrm{Tr}(\chi_+)$, and traceless $\tilde{\chi}_+$. The LECs in $\mathcal{L}_{4H}^{(2,h)}$ and $\mathcal{L}_{4H}^{(2,d)}$ will absorb the divergent parts from the one-loop diagrams that are proportional to m_ϕ^2. $\mathcal{L}_{4H}^{(2,v)}$ will absorb the divergent parts proportional to the square of the external line energy. There are also divergent parts proportional to the mass difference Δ, which will vanish in the heavy meson symmetry limit. These divergences can be absorbed by the additional four heavy meson interaction terms proportional to Δ. $\mathcal{L}_{4H}^{(2,q)}$ does not contribute to the renormalization of the $\bar{B}\bar{B}$ potentials. Instead it will contribute to the $\bar{B}\bar{B}^*$ and $\bar{B}^*\bar{B}^*$ potentials.

III. POTENTIALS WITH HMχPT

With the strict isospin symmetry, there are only four independent potentials for the channels $\bar{B}\bar{B}^1$, $\bar{B}\bar{B}^0$, $\bar{B}_s\bar{B}_s{}^0$, and $\bar{B}\bar{B}_s{}^{1/2}$. The superscript represents the isospin of the channel. At the leading order, the potentials of the bottomed mesons only receive the contributions from the tree diagrams with the contact terms in $\mathcal{L}_{4H}^{(0)}$,

$$V^{(0)}_{\bar{B}\bar{B}^1} = -2D_a - \frac{8}{3}E_a, \qquad V^{(0)}_{\bar{B}\bar{B}^0} = 0,$$
$$V^{(0)}_{\bar{B}_s\bar{B}_s{}^0} = -2D_a - \frac{8}{3}E_a, \qquad V^{(0)}_{\bar{B}\bar{B}_s{}^{1/2}} = -2D_a - \frac{8}{3}E_a. \quad (14)$$

The loop diagrams in Figs. 2 and 3 will contribute at the next to leading order. The diagrams h.1, h.2, and B.1 in Figs. 2 and 3 contain both 2PR and 2PI parts if using the ordinary Feynman rules of HMχPT. We must remove the 2PR contribution to get the correct potentials. The 2PR parts result from the double poles of the two heavy mesons, which can be removed by the careful subtraction in the propagator of the heavy mesons

$$\frac{1}{[v\cdot p_1+\delta_1+i\varepsilon][v\cdot p_2+\delta_2+i\varepsilon]} = \begin{cases} \frac{1}{v\cdot p_1+\delta_1+i\varepsilon}\left[\frac{-1}{v\cdot p_1+\delta_1+i\varepsilon} - 2\pi i\delta(v\cdot p_1+\delta_1)\right] \to \frac{-1}{(v\cdot p_1+\delta_1+i\varepsilon)^2} & v\cdot p_2+\delta_2 = -v\cdot p_1-\delta_1 \\ \frac{1}{[v\cdot p_1+\delta_1+i\varepsilon][v\cdot p_2+\delta_2+i\varepsilon]} & \text{other} \end{cases}. \quad (15)$$

We calculate these Feynman diagrams with dimension regularization and the modified minimal subtraction scheme. The divergent terms proportional to L will be absorbed by the contact terms at $O(\epsilon^2)$, where

$$L = \frac{\lambda^{D-4}}{16\pi^2}\left\{\frac{1}{D-4} + \frac{1}{2}(\gamma_E - 1 - \ln 4\pi)\right\}. \quad (16)$$

Here γ_E is the Euler constant 0.5772157, λ is the scale of the dimension regularization, and we set $\lambda = 4\pi f$.

The potentials are finite after the renormalization of the wave functions and vertices. The diagram z.1 in Fig. 2 arises from the renormalization of the wave functions. The combined divergence generated by diagrams g.1 and g.2 in Fig. 2 can be absorbed by the LECs D_{ai}^v, E_{ai}^v, $D_b^{h/d}$, and $E_b^{h/d}$. The divergence generated by the diagram h.1 or h.2 can be absorbed by the redefinitions of LECs in $\mathcal{L}_{4H}^{(2,h)}$, $\mathcal{L}_{4H}^{(2,d)}$, and $\mathcal{L}_{4H}^{(2,v)}$. For the 2ϕ exchange diagrams in Fig. 3, the divergence of the football or triangle diagram can be absorbed by E_{ai}^v and $E_a^{h/d}$. The divergence of the box and crossed diagram can be absorbed by D_{ai}^v, $D_a^{h/d}$, E_{ai}^v, and $E_a^{h/d}$.

The potentials obtained from the same Feynman diagram for the different channels differ just by a flavor dependent

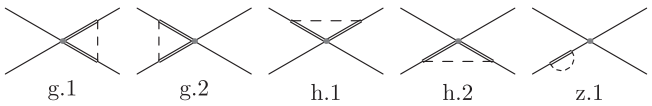

FIG. 2. The loop diagrams with a contact vertex. The thin solid, thick solid, and dashed lines represent the heavy pseudoscalar mesons, heavy vector mesons, and light pseudoscalar mesons, respectively.

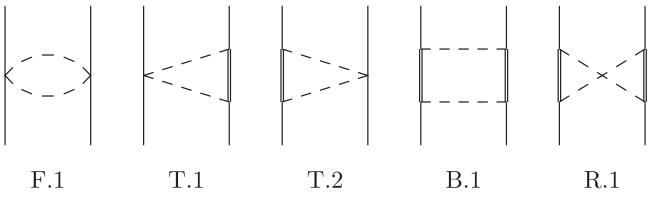

FIG. 3. The 2ϕ-exchange diagrams including the football diagram (F.1), triangle diagrams (T.1 and T.2), box diagram (B.1), and crossed diagram (R.1).

coefficient. So it is convenient to write down the potential of the channel "ch" in the form

$$V_{ch}^{(2)} = -\frac{1}{4}\sum_{\text{diag},m_1,m_2,\ldots}\beta^{\text{diag}}{}_{ch}(m_1,m_2,\ldots) \otimes Y^{\text{diag}}(m_1,m_2,\ldots), \tag{17}$$

where "diag" runs over all the Feynman diagrams shown in Figs. 2 and 3, and m_i runs over $\{m_\pi, m_K, m_\eta\}$. Y is a scalar function independent of the flavor structure of the channel ch, while β is the flavor dependent coefficient.

The corresponding Y functions of Fig. 2 are

$$Y^{g.1}(m) \equiv -\frac{g^2}{f^2}\left\{\left[\frac{D}{4}-\frac{1}{4}\right]J_{22}^{g}\right\}_r(m,\mathcal{E}-q_0-\Delta,\mathcal{E}-\Delta), \tag{18}$$

$$Y^{g.2}(m) \equiv -\frac{g^2}{f^2}\left\{\left[\frac{D}{4}-\frac{1}{4}\right]J_{22}^{g}\right\}_r(m,\mathcal{E}+q_0-\Delta,\mathcal{E}-\Delta), \tag{19}$$

$$Y^{h.1}(m) \equiv -\frac{g^2}{f^2}\left\{\left[\frac{D}{4}-\frac{1}{4}\right]J_{22}^{h}\right\}_r(m,\mathcal{E}-\Delta,\mathcal{E}-\Delta), \tag{20}$$

$$Y^{h.2}(m) \equiv -\frac{g^2}{f^2}\left\{\left[\frac{D}{4}-\frac{1}{4}\right]J_{22}^{h}\right\}_r(m,\mathcal{E}-q_0-\Delta,\mathcal{E}+q_0-\Delta), \tag{21}$$

$$Y^{z.1}(m) \equiv \frac{g^2}{f^2}\left\{\left[\frac{D}{4}-\frac{1}{4}\right]\partial_x J_{22}^{a}\right\}_r(m,x)\Big|_{x\to-\Delta}, \tag{22}$$

where we work in the center-of-mass frame of the incoming heavy mesons, $\mathcal{E}$ is the residual energy of the incoming heavy meson (the difference between the energy and the $\bar{B}$ meson mass), and q is the transferred momentum. The definitions of the J functions are collected in Appendix A. $\{X\}_r$ represents the finite part of X,

$$\{X\}_r = \lim_{D\to4}\left(X - L\frac{\partial}{\partial L}X\right) + \frac{1}{16\pi^2}\lim_{D\to4}\left(\frac{\partial}{\partial D}\frac{\partial}{\partial L}X\right). \tag{23}$$

The loop diagrams in Fig. 2 are made up of the contact vertices of $\mathcal{L}_{4H}^{(0)}$, so the flavor dependent coefficient β can be written down as

$$\beta = D_a\tilde{\beta}_{\text{Da}} + D_b\tilde{\beta}_{\text{Db}} + E_a\tilde{\beta}_{\text{Ea}} + E_b\tilde{\beta}_{\text{Eb}}. \tag{24}$$

Actually, only three coefficient βs for the diagrams g.1, h.1, and z.1 in Fig. 2 are independent. For convenience, we list $\{\tilde{\beta}_{\text{Da}}^{g.1},\tilde{\beta}_{\text{Da}}^{z.1},\tilde{\beta}_{\text{Db}}^{g.1},\tilde{\beta}_{\text{Db}}^{h.1}\}$ in Table I and $\{\tilde{\beta}_{\text{Ea}}^{g.1},\tilde{\beta}_{\text{Ea}}^{z.1},\tilde{\beta}_{\text{Eb}}^{g.1},\tilde{\beta}_{\text{Eb}}^{h.1}\}$ in Table II. The coefficient βs for g.2 and h.2 can be obtained by the following relations:

$$\begin{aligned}&\tilde{\beta}_{\text{Da}}^{g.2} = \tilde{\beta}_{\text{Da}}^{g.1}, \quad \tilde{\beta}_{\text{Db}}^{g.2} = \tilde{\beta}_{\text{Db}}^{g.1}, \quad \tilde{\beta}_{\text{Db}}^{h.2} = \tilde{\beta}_{\text{Db}}^{h.1},\\ &\tilde{\beta}_{\text{Ea}}^{g.2} = \tilde{\beta}_{\text{Ea}}^{g.1}, \quad \tilde{\beta}_{\text{Eb}}^{g.2} = \tilde{\beta}_{\text{Eb}}^{g.1}, \quad \tilde{\beta}_{\text{Eb}}^{h.2} = \tilde{\beta}_{\text{Eb}}^{h.1},\end{aligned} \tag{25}$$

and all the others are zero.

Now one can write down the potentials induced by Fig. 2 for the different channels. Let us take the $\bar{B}\bar{B}^0$ system as an example. One can get the contribution from the diagram g.1 by Tables I and II,

TABLE I. The coefficient βs of the loop diagrams with a contact term: $\{\tilde{\beta}_{\text{Da}}^{g.1},\tilde{\beta}_{\text{Da}}^{z.1},\tilde{\beta}_{\text{Db}}^{g.1},\tilde{\beta}_{\text{Db}}^{h.1}\}$.

0	(m_π)	(m_K)	(m_η)
$\bar{B}\,\bar{B}^1$	$\{24,-48,-8,-8\}$	$\{16,-32,0,0\}$	$\{\frac{8}{3},-\frac{16}{3},-\frac{8}{3},-\frac{8}{3}\}$
$\bar{B}\,\bar{B}^0$	$\{24,0,-24,0\}$	$\{16,\ 0,\ 0,\ 0\}$	$\{\frac{8}{3},0,\frac{8}{3},0\}$
$\bar{B}_s\bar{B}_s{}^0$	0	$\{32,-64,0,0\}$	$\{\frac{32}{3},-\frac{64}{3},-\frac{32}{3},-\frac{32}{3}\}$
$\bar{B}\bar{B}_s{}^{1/2}$	$\{12,-24,0,0\}$	$\{24,-48,-16,-16\}$	$\{\frac{20}{3},-\frac{40}{3},\frac{16}{3},\frac{16}{3}\}$

TABLE II. The coefficient βs of the loop diagrams with a contact term: $\{\tilde{\beta}_{\text{Ea}}^{g.1},\tilde{\beta}_{\text{Ea}}^{z.1},\tilde{\beta}_{\text{Eb}}^{g.1},\tilde{\beta}_{\text{Eb}}^{h.1}\}$.

0	(m_π)	(m_K)	(m_η)
$\bar{B}\,\bar{B}^1$	$\{0,-64,-\frac{128}{3},-\frac{32}{3}\}$	$\{-\frac{32}{3},-\frac{128}{3},-32,0\}$	$\{\frac{32}{9},-\frac{64}{9},-\frac{32}{9},-\frac{32}{9}\}$
$\bar{B}\,\bar{B}^0$	$\{32,0,-32,0\}$	$\{-\frac{32}{3},0,-32,0\}$	$\{-\frac{64}{9},0,-\frac{64}{9},0\}$
$\bar{B}_s\bar{B}_s{}^0$	0	$\{-\frac{64}{3},-\frac{256}{3},-64,0\}$	$\{\frac{128}{9},-\frac{256}{9},-\frac{128}{9},-\frac{128}{9}\}$
$\bar{B}\bar{B}_s{}^{1/2}$	$\{-8,-32,-24,0\}$	$\{16,-64,-\frac{112}{3},-\frac{64}{3}\}$	$\{-\frac{136}{9},-\frac{160}{9},-\frac{152}{9},\frac{64}{9}\}$

TABLE III. The coefficient βs of the 2-ϕ exchange diagrams: $\{\beta^{B.1}, \beta^{R.1}\}$.

	(m_π, m_π)	(m_K, m_K)	(m_η, m_η)	(m_π, m_K)	(m_π, m_η)	(m_K, m_η)	(m_K, m_π)	(m_η, m_π)	(m_η, m_K)
$\bar{B}\bar{B}^1$	$\{-1,-5\}$	$\{0,-4\}$	$\{-\frac{1}{9},-\frac{1}{9}\}$	0	$\{-\frac{1}{3},-\frac{1}{3}\}$	0	0	$\{-\frac{1}{3},-\frac{1}{3}\}$	0
$\bar{B}\bar{B}^0$	$\{-9,3\}$	$\{0,4\}$	$\{-\frac{1}{9},-\frac{1}{9}\}$	0	$\{1,1\}$	0	0	$\{1,1\}$	0
$\bar{B}_s\bar{B}_s{}^0$	0	$\{0,-8\}$	$\{-\frac{16}{9},-\frac{16}{9}\}$	0	0	0	0	0	0
$\bar{B}\bar{B}_s{}^{1/2}$	0	$\{-4,0\}$	$\{-\frac{4}{9},-\frac{4}{9}\}$	$\{0,-3\}$	0	$\{\frac{4}{3},-\frac{5}{3}\}$	$\{0,-3\}$	0	$\{\frac{4}{3},-\frac{5}{3}\}$

$$V^{g.1}_{\bar{B}\bar{B}^0} = -\frac{1}{4}[24D_a - 24D_b + 32E_a - 32E_b]Y^{g.1}(m_\pi) - \frac{1}{4}\left[16D_a - \frac{32}{3}E_a - 32E_b\right]Y^{g.1}(m_K) - \frac{1}{4}\left[\frac{8}{3}D_a + \frac{8}{3}D_b - \frac{64}{9}E_a - \frac{64}{9}E_b\right]Y^{g.1}(m_\eta). \tag{26}$$

The diagrams in Fig. 3 represent the potentials with the 2ϕ exchange. We list the β functions $\{\beta^{B.1}, \beta^{R.1}\}$ in Table III, and all the others can be obtained by the following relations:

$$\beta^{F.1} = \frac{-\beta^{B.1} + \beta^{R.1}}{16}, \qquad \beta^{T.1} = \beta^{T.2} = \frac{-\beta^{B.1} + \beta^{R.1}}{4}. \tag{27}$$

The corresponding Y functions of Fig. 3 are

$$Y^{F.1}(m,M) \equiv \frac{1}{f^4}\{J^F_{22} + [q_0^2]J^F_0 + [4q_0^2]J^F_{11} + [4q_0^2]J^F_{21}\}_r(m,M,q), \tag{28}$$

$$Y^{T.1}(m,M) \equiv \frac{g^2}{f^4}\left\{J^T_{34} + \left[\frac{Dq_0}{2} - \frac{q_0}{2}\right]J^T_{21} + [Dq_0 - q_0]J^T_{31} + [-\vec{q}^2]J^T_{24} + [-\vec{q}^2]J^T_{33} + \left[-\frac{1}{2}q_0\vec{q}^2\right]J^T_{11} + \left[-\frac{3}{2}q_0\vec{q}^2\right]J^T_{22} + [-q_0\vec{q}^2]J^T_{32}\right\}_r(m,M,\mathcal{E}+q_0-\Delta,q), \tag{29}$$

$$Y^{T.2}(m,M) \equiv \frac{g^2}{f^4}\left\{J^T_{34} + \left[\frac{Dq_0}{2} - \frac{q_0}{2}\right]J^T_{21} + [Dq_0 - q_0]J^T_{31} + [-\vec{q}^2]J^T_{24} + [-\vec{q}^2]J^T_{33} + \left[-\frac{1}{2}q_0\vec{q}^2\right]J^T_{11} + \left[-\frac{3}{2}q_0\vec{q}^2\right]J^T_{22} + [-q_0\vec{q}^2]J^T_{32}\right\}_r(m,M,\mathcal{E}-\Delta,q), \tag{30}$$

$$Y^{B.1}(m,M) \equiv \frac{g^4}{f^4}\left\{\left[\frac{D^2}{4} - \frac{1}{4}\right]J^B_{41} + \left[-\frac{1}{4}\vec{q}^2\right]J^B_{21} + \left[-\frac{1}{2}D\vec{q}^2 - \frac{1}{2}\vec{q}^2\right]J^B_{31} + \left[-\frac{1}{2}D\vec{q}^2 - \frac{1}{2}\vec{q}^2\right]J^B_{42} + \left[\frac{1}{4}(\vec{q}^2)^2\right]J^B_{22} + \left[\frac{1}{2}(\vec{q}^2)^2\right]J^B_{32} + \left[\frac{1}{4}(\vec{q}^2)^2\right]J^B_{43}\right\}_r(m,M,\mathcal{E}-\Delta,\mathcal{E}-\Delta,q), \tag{31}$$

$$Y^{R.1}(m,M) \equiv \frac{g^4}{f^4}\left\{\left[\frac{D^2}{4} - \frac{1}{4}\right]J^R_{41} + \left[-\frac{1}{4}\vec{q}^2\right]J^R_{21} + \left[-\frac{1}{2}D\vec{q}^2 - \frac{1}{2}\vec{q}^2\right]J^R_{31} + \left[-\frac{1}{2}D\vec{q}^2 - \frac{1}{2}\vec{q}^2\right]J^R_{42} + \left[\frac{1}{4}(\vec{q}^2)^2\right]J^R_{22} + \left[\frac{1}{2}(\vec{q}^2)^2\right]J^R_{32} + \left[\frac{1}{4}(\vec{q}^2)^2\right]J^R_{43}\right\}_r(m,M,\mathcal{E}-\Delta,\mathcal{E}+q_0-\Delta,q). \tag{32}$$

Again, taking the $\bar{B}\bar{B}^0$ channel as an example, the potential from the diagram B.1 of Fig. 3 reads

$$V^{B.1}_{\bar{B}\bar{B}^0} = -\frac{1}{4}\left[-9Y^{B.1}(m_\pi,m_\pi) - \frac{1}{9}Y^{B.1}(m_\eta,m_\eta) + Y^{B.1}(m_\pi,m_\eta) + Y^{B.1}(m_\eta,m_\pi)\right]. \tag{33}$$

Finally, the potentials $V^{(2)}$ at $O(\epsilon^2)$ can be obtained by summing the products of the corresponding β and Y as in Eq. (17).

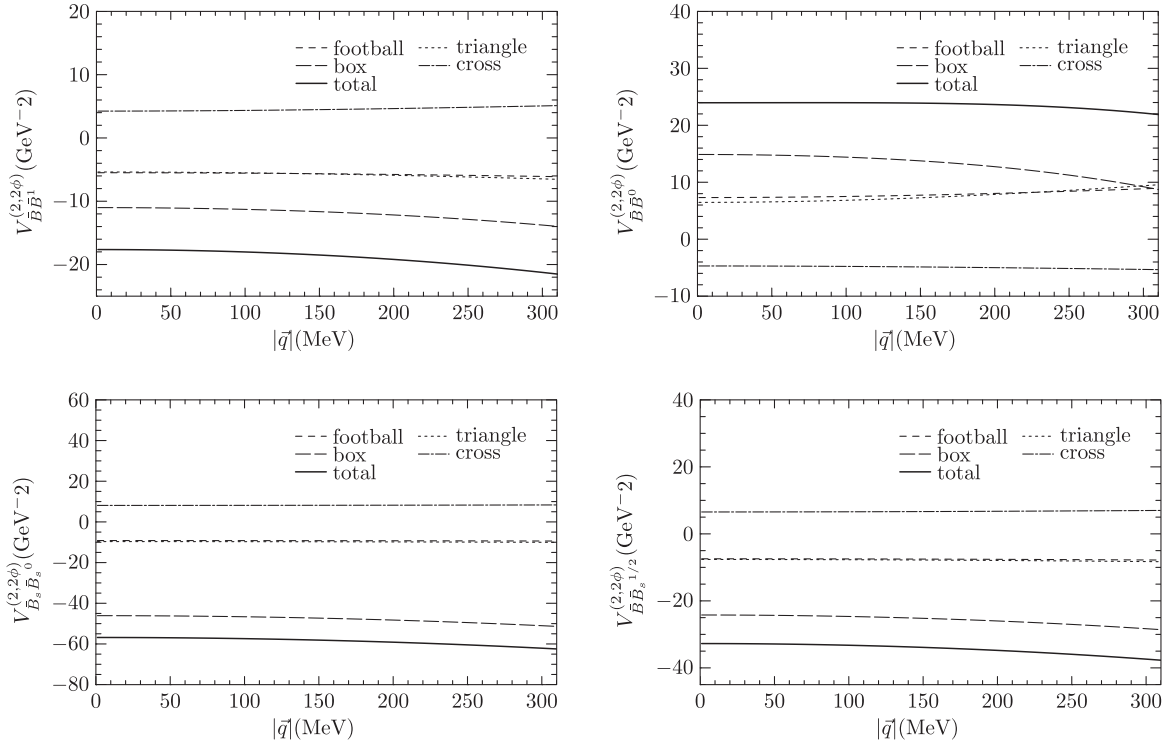

FIG. 4. The $\bar{B}\,\bar{B}$ potentials with the 2ϕ exchange.

IV. NUMERICAL RESULTS AND DISCUSSIONS

A. Potentials of $\bar{B}\,\bar{B}$ mesons

We have calculated the potentials of $\bar{B}\,\bar{B}$ mesons up to $O(\epsilon^2)$ for four independent channels. The $O(\epsilon^2)$ potentials $V^{(2)}$ contain two parts $V^{(2,\mathrm{cont})}$ and $V^{(2,2\phi)}$, corresponding to Figs. 2 and 3, respectively. We will focus on the potentials with $\mathcal{E} = q^0 = 0$ in the momentum space. After the Fourier transformation, we can get the traditional potentials in the coordinate space. The other parameters are listed as follows [38–41]:

$$m_\pi = 139\ \mathrm{MeV}, \qquad m_K = 494\ \mathrm{MeV},$$
$$m_\eta = \sqrt{(4m_K^2 - m_\pi^2)/3}, \qquad \Delta = 46\ \mathrm{MeV},$$
$$f = 92\ \mathrm{MeV}, \qquad g = 0.52, \tag{34}$$

where Δ is the mass difference between $\bar{B}$ and $\bar{B}^*$ mesons, f is the pion decay constant, and g is the axial coupling constant from the unquenched lattice QCD simulation.

The potentials $V^{(0)}$ and $V^{(2,\mathrm{cont})}$ are both generated by the contact vertices. They are independent of the transferred momentum $|\vec{q}|$. They are $\delta(\vec{r})$-like potentials in the coordinate space. From Eq. (14), we notice that the terms proportional to D_b and E_b in $\mathcal{L}^{(0)}_{4H}$ do not contribute to $V^{(0)}$. The potential vanishes in the channel $(\bar{B}\,\bar{B})^0$ at the leading order. At the next to leading order, the situation is different,

$$V^{(2,\mathrm{cont})}_{\bar{B}\,\bar{B}^1} = -0.32E_a - 0.32E_b,$$
$$V^{(2,\mathrm{cont})}_{\bar{B}\,\bar{B}^0} = 0.19D_a - 0.02D_b - 0.085E_a - 0.36E_b,$$
$$V^{(2,\mathrm{cont})}_{\bar{B}_s\bar{B}_s{}^0} = -0.53E_a - 0.53E_b,$$
$$V^{(2,\mathrm{cont})}_{\bar{B}\bar{B}_s{}^{1/2}} = -0.32E_a - 0.32E_b. \tag{35}$$

All the terms in $\mathcal{L}^{(0)}_{4H}$ contribute to $V^{(2,\,\mathrm{cont})}$. However, in the $\bar{B}\,\bar{B}^1$, $\bar{B}_s\bar{B}_s{}^0$, and $\bar{B}\bar{B}_s{}^{1/2}$ channels, the contributions proportional to D_a or D_b from different diagrams in Fig. 2 cancel each other. Roughly speaking, the corrections $V^{(2,\mathrm{cont})}$ are small compared with the leading order contribution. We also notice that

$$|V^{(2,\mathrm{cont})}_{\bar{B}_s\bar{B}_s{}^0}| > |V^{(2,\mathrm{cont})}_{\bar{B}\bar{B}_s{}^{1/2}}| \approx |V^{(2,\mathrm{cont})}_{\bar{B}\,\bar{B}^1}|. \tag{36}$$

As we have emphasized in the previous section, the finite parts of the $O(\epsilon^2)$ LECs in Eqs. (9)–(12) also contribute to the potential while its divergent parts cancel the divergence from the one-loop diagrams. Unfortunately, we are unable to fix these LECs because of the lack of experimental data. In the following analysis, we focus on the behavior of the 2ϕ-exchange potentials.

We plot the 2ϕ-exchange potentials $V^{(2,2\phi)}$ of the $\bar{B}\,\bar{B}$ mesons in Fig. 4. From the figure, the contributions from the football and triangle diagrams are coincidentally close in all the $\bar{B}\,\bar{B}$ channels. When the transferred momentum is small, the sign of the potential from the crossed diagrams is

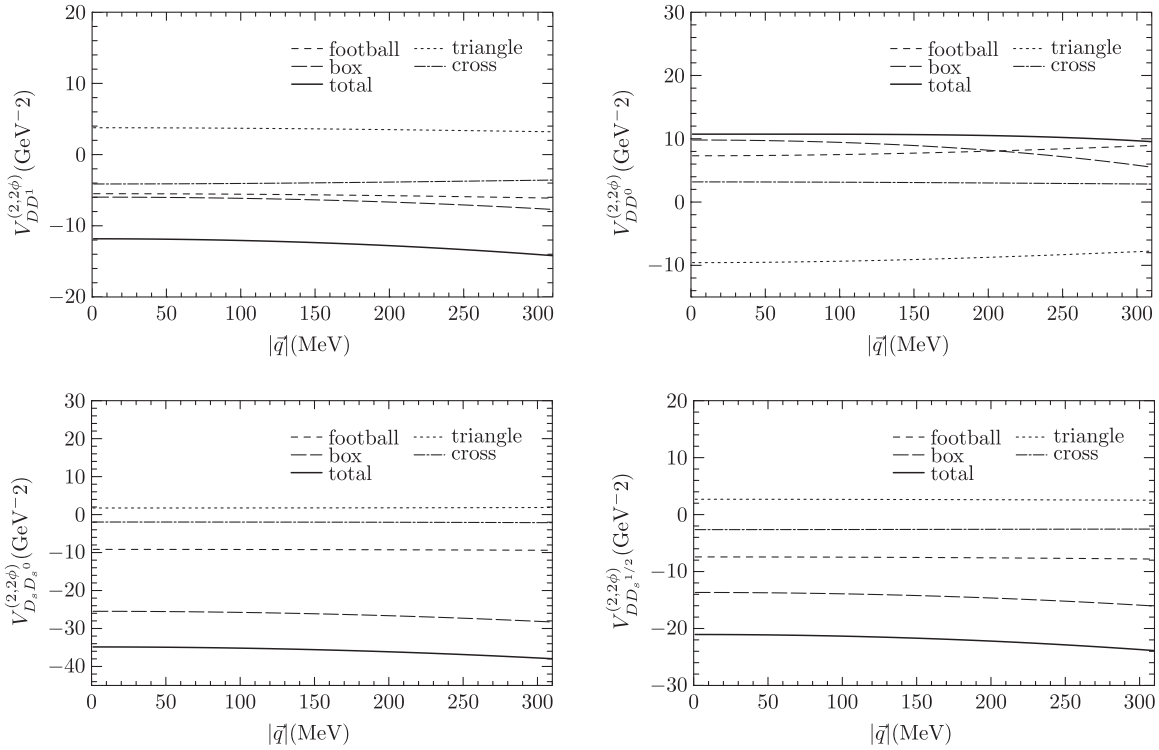

FIG. 5. The DD potentials with the 2ϕ exchange.

different from that of the other 2ϕ-exchange diagrams. We have noticed that the 2ϕ-exchange potentials of the $\bar{B}\bar{B}^1$, $\bar{B}_s\bar{B}_s{}^0$, and $\bar{B}\bar{B}_s{}^{1/2}$ channels are negative in the small-momentum region. In other words, the 2ϕ-exchange interaction is attractive if we ignore the contribution from the LECs. In contrast, the 2ϕ-exchange interaction of the $\bar{B}\bar{B}^0$ channel is repulsive in the small-momentum region without these LECs. The 2ϕ-exchange potential in the $\bar{B}_s\bar{B}_s{}^0$ channel is nearly twice as large as those in the other channels.

The potentials from the football diagram, triangle diagram, box diagram, and crossed diagram are proportional to g^0, g^2, g^4, and g^4, respectively, from Eqs. (28)–(32). So because the coupling constant $g = 0.52$ is quite small, one would naively expect that the potential from the triangle diagram is suppressed by a factor of about 0.27, and the potential from the box or cross diagram is suppressed by about 0.07 compared with that from the football diagram. However, we do not see the suppression in Fig. 4. There is also an enhancement of the flavor coefficient β for the triangle, box, and crossed diagram from Eq. (27), which roughly compensates for the suppression of the small g. That is why we see neither the suppression due to the small g nor the enhancement of β in the numerical results. If we let $g \to 1$, the potential from the box or crossed diagram would be much larger than the potential from the triangle diagram, which would be larger than the potential from the football diagram.

From Fig. 4, we notice that the contribution from the box diagram dominates the potential $V^{(2,2\phi)}$. From Eq. (32), we have

$$15 \lessapprox \frac{Y^{B.1}(m_{\phi_1}, m_{\phi_2})}{Y^{B.1}(m_\pi, m_\pi)} \lessapprox 50, \tag{37}$$

where the intermediate meson pair $\phi_1\phi_2$ can be πK, $\pi\eta$, KK, $K\eta$, or $\eta\eta$. So the potential from the box diagram is dominated by the intermediate states with at least one kaon or eta meson.

B. Potentials of the DD mesons

Similarly we can study the potentials between the D^0, D^+, and D_s^+ mesons. Now the intermediate heavy vector mesons are D^{*0}, D^{*+}, and D_s^{*+}. The mass difference Δ increases to 142 MeV. The axial coupling constant $g = 0.59$ from the decay width of D^{*+} [38]. The LECs D_a, E_a, etc., should be modified correspondingly. The expressions for the DD mesons are the same as those for the $\bar{B}\bar{B}$'s except that the channels are DD^1, DD^0, $D_sD_s{}^0$, and $DD_s{}^{1/2}$. The DD potentials with the 2ϕ exchange are plotted in Fig. 5. The potentials related to the contact terms are

$$\begin{aligned}
V^{(2,\mathrm{cont})}_{DD^1} &= 0.89E_a^{DD} + 0.89E_b^{DD},\\
V^{(2,\mathrm{cont})}_{DD^0} &= -0.59D_a^{DD} + 0.2D_b^{DD} - 0.0056E_a^{DD} + 1.1E_b^{DD},\\
V^{(2,\mathrm{cont})}_{D_sD_s{}^0} &= 1.1E_a^{DD} + 1.1E_b^{DD},\\
V^{(2,\mathrm{cont})}_{DD_s{}^{1/2}} &= 1.1E_a^{DD} + 1.1E_b^{DD}.
\end{aligned} \tag{38}$$

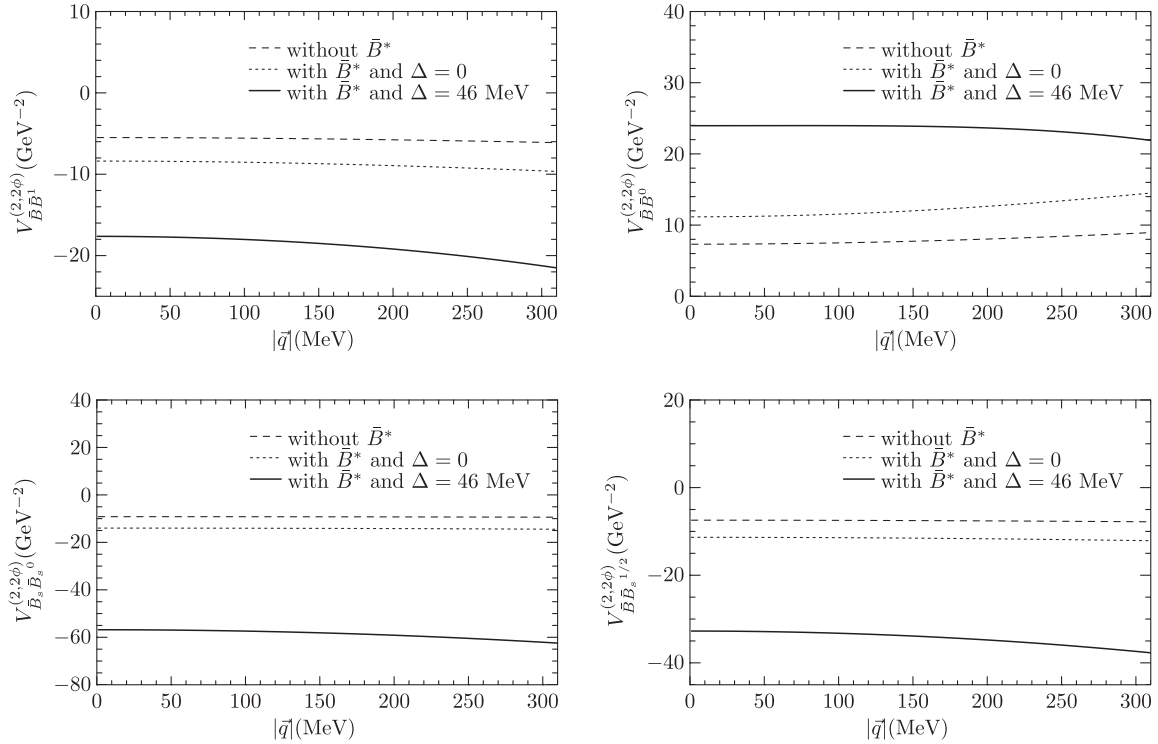

FIG. 6. The $\bar{B}\,\bar{B}$ potentials with the 2ϕ exchange in different schemes.

We notice that there is a big difference between the potentials $V^{(2,\mathrm{cont})}$ of the $\bar{B}\,\bar{B}$ and DD mesons by comparing Eqs. (35) and (38). The difference originates from the different axial coupling g and mass difference Δ. The signs of most of the terms in $V^{(2,\mathrm{cont})}$ are different for the bottom and charm cases if assuming $D^{DD}_{a/b}$ ($E^{DD}_{a/b}$) is equal to $D_{a/b}$ ($E_{a/b}$) for the $\bar{B}$ mesons. One obtains the relation

$$|V^{(2,\mathrm{cont})}_{DD_s{}^{1/2}}| \approx |V^{(2,\mathrm{cont})}_{D_sD_s{}^0}| > |V^{(2,\,\mathrm{cont})}_{DD^1}|, \tag{39}$$

which is different from that in the case of the $\bar{B}$ mesons.

Comparing Figs. 4 and 5, one can find that the total $V^{(2,2\phi)}_{\bar{B}\,\bar{B}}$ is roughly twice $V^{(2,2\phi)}_{DD}$ for each channel. Moreover, the separate contributions from the crossed or triangle diagrams have opposite signs for the $\bar{B}$ and D mesons.

One can obtain the potentials of anti-heavy mesons based on C-parity conservation

$$V_{BB'} = V_{\bar{B}\,\bar{B}'}, \qquad V_{\bar{D}\,\bar{D}'} = V_{DD'}. \tag{40}$$

V. COMPARISON BETWEEN RESULTS IN DIFFERENT SCHEMES

One can also systematically study the potentials of the heavy pseudoscalar mesons without heavy vector mesons as the explicit degrees. The contributions from the heavy vector mesons, as well as other resonances, will be embodied in the low-energy constants. In the scheme without heavy vector mesons, the potential at the leading order remains the same. However, only the football diagram survives at $O(\epsilon^2)$.

It is also very interesting to investigate the case with strict heavy quark spin symmetry. Now the heavy vector mesons are included as the explicit degrees but the mass difference Δ is set to be zero. When Δ approaches 0, the potentials induced by the diagrams h.1, h.2, and B.1 will approach infinity if the 2PR contributions are not removed. The two-heavy-vector-meson-reducible contribution does not appear when the mass difference Δ is finite. It only appears as $\Delta = 0$ before the subtraction. So there is a jump in the potentials as Δ goes from nonzero to zero. When solving the nonperturbative equation to get the observable, the potentials such as $V_{\bar{B}\,\bar{B}\to\bar{B}^*\bar{B}^*}$ must be included as $\Delta = 0$. But they are not necessary as $\Delta \neq 0$. Thus the jump might vanish for the observable such as the binding energy.

In the new approximations, the potentials do not change at the leading order. The difference appears at the next to leading order. In the approximation without the heavy vector mesons, there does not exist those diagrams in Fig. 2, so $V^{(2,\mathrm{cont})} = 0$. In the approximation including the heavy vector mesons and $\Delta = 0$, we have

$$\begin{aligned}
V^{(2,\mathrm{cont})}_{\bar{B}\,\bar{B}^1} &= -0.78E_a - 0.78E_b,\\
V^{(2,\mathrm{cont})}_{\bar{B}\,\bar{B}^0} &= 0.48D_a - 0.077D_b - 0.17E_a - 0.91E_b,\\
V^{(2,\mathrm{cont})}_{\bar{B}_s\bar{B}_s{}^0} &= -1.2E_a - 1.2E_b,\\
V^{(2,\mathrm{cont})}_{\bar{B}\bar{B}_s{}^{1/2}} &= -0.88E_a - 0.88E_b,
\end{aligned} \tag{41}$$

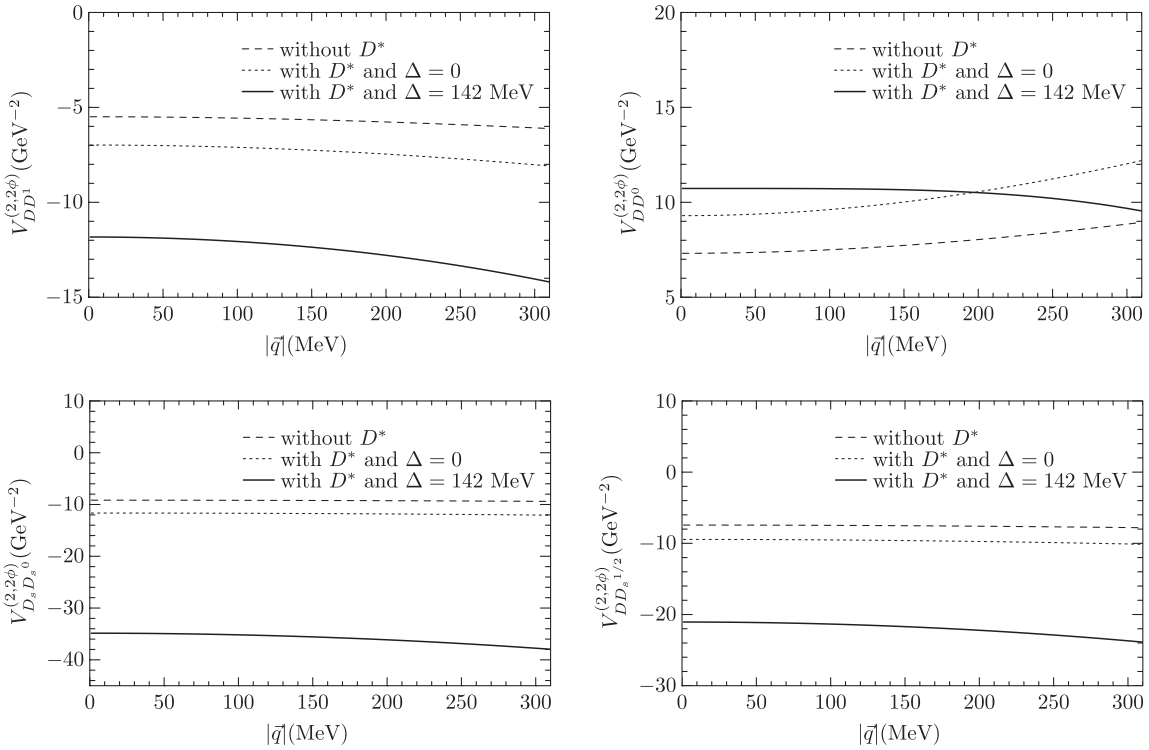

FIG. 7. The DD potentials with the 2ϕ exchange in different schemes.

and

$$V^{(2,\mathrm{cont})}_{DD^1} = -1.0E^{DD}_a - 1.0E^{DD}_b,$$
$$V^{(2,\mathrm{cont})}_{DD^0} = 0.62D^{DD}_a - 0.099D^{DD}_b - 0.22E^{DD}_a - 1.2E^{DD}_b,$$
$$V^{(2,\mathrm{cont})}_{D_sD_s{}^0} = -1.6E^{DD}_a - 1.6E^{DD}_b,$$
$$V^{(2,\mathrm{cont})}_{DD_s{}^{1/2}} = -1.1E^{DD}_a - 1.1E^{DD}_b. \quad (42)$$

The difference between the $\bar{B}\bar{B}$ and DD potentials only originates from the different axial coupling g as $\Delta = 0$,

$$\frac{V^{(2,\mathrm{cont})}_{\bar{B}\bar{B}}}{V^{(2,\mathrm{cont})}_{DD}} = \frac{0.52^2}{0.59^2} = 0.8, \quad \text{for } \Delta = 0. \quad (43)$$

The $\bar{B}\bar{B}$ potential with $\Delta = 0$ is nearly twice as large as that with $\Delta = 46$ MeV in every channel by comparing Eqs. (35) and (41). The potentials with $\Delta = 46$ MeV are approximately equal in the channels $\bar{B}\bar{B}^1$ and $\bar{B}\bar{B}_s{}^{1/2}$, while those with $\Delta = 0$ are not equal. The difference between the DD potentials is even larger with different Δ from Eqs. (38) and (42). The sign of the DD potential as $\Delta = 0$ is different from that as $\Delta = 142$ MeV in every channel. The potential of the channel $D_sD_s{}^0$ is very close to that of the channel $DD_s{}^{1/2}$ for the case with $\Delta = 142$ MeV, but the situation is different for the case with $\Delta = 0$.

The difference between the potentials with different Δ mainly results from the subtraction of the 2-heavy-vector-meson-reducible contributions to get the potentials of the heavy pseudoscalar mesons as $\Delta = 0$. To recover the two-heavy-vector-meson-reducible contributions, one should include the potentials such as $V_{\bar{B}\bar{B}\to\bar{B}^*\bar{B}^*}$ when solving the nonperturbative equations to get the observable as $\Delta = 0$.

We list the $\bar{B}\bar{B}$ and DD potentials with 2ϕ exchange in different approximations in Figs. 6 and 7, respectively. From Fig. 6, the potentials are relatively close between the case without $\bar{B}^*$ (case I) and that with $\Delta = 0$ (case II). The potential $|V|$ for case I or II is about 15%–50% of that for the case with $\bar{B}^*$ and $\Delta = 46$ MeV (case III) in every channel. The dependence of the potential on $|\vec{q}|$ for case III

TABLE IV. The 2ϕ-exchange potentials of $\bar{B}\bar{B}$ with different λ in units of GeV^{-2}.

	$V^{(2,2\phi)}_{\bar{B}\bar{B}^1}$		$V^{(2,2\phi)}_{\bar{B}\bar{B}^0}$		$V^{(2,2\phi)}_{\bar{B}_s\bar{B}_s{}^0}$		$V^{(2,2\phi)}_{\bar{B}\bar{B}_s{}^{1/2}}$	
$\lvert\vec{q}\rvert$ [MeV]	0	300	0	300	0	300	0	300
$\lambda = 4\pi f$	−18	−21	24	22	−57	−62	−33	−37
$\lambda = 0.8$ GeV	−14	−18	20	18	−51	−56	−28	−32

is slightly stronger than that for the other two cases in the channels $\bar{B}\bar{B}^1$, $\bar{B}_s\bar{B}_s{}^0$, and $\bar{B}\bar{B}_s{}^{1/2}$. The potential decreases for case III and increases for the other two cases as $|\vec{q}|$ grows in the channel $\bar{B}\bar{B}^0$.

The situation in Fig. 7 is similar to that in Fig. 6. But the difference of the DD potentials between different cases is smaller than that of the $\bar{B}\bar{B}$ potentials. We notice that the DD potential is equal to the $\bar{B}\bar{B}$ potential for case I in each channel since the potential from the football diagram is independent of the mass difference Δ and the axial coupling constant g.

The 2ϕ-exchange potentials in our results depend on the energy scale λ that arises from the dimensional regularization. Thus the variations of the potentials with λ might reveal the effect of the LECs to some extent. We reset $\lambda = 0.8$ GeV, which is different from the previous one $\lambda = 4\pi f \approx 1.2$ GeV. For comparison, we list $V^{(2,2\phi)}_{\bar{B}\bar{B}}$ potentials (for case III) with different λ in Table IV. From Table IV, one notices that as λ goes from $4\pi f$ to 0.8 GeV, the 2ϕ-exchange potential changes about 10%–20%.

VI. SUMMARY

In a short summary, we have calculated the potentials of the heavy pseudoscalar mesons up to $O(\epsilon^2)$ in the momentum space with HMχPT. We have carefully analyzed the tree-level contribution and one-loop correction to the contact vertices, and the 2π-exchange contribution. We have also discussed the potentials in different schemes.

Generally speaking, the potential of hadrons can be separated into long-range, medium-range, and short-range parts. For the two heavy pseudoscalar mesons, there does not exist the long-range 1ϕ-exchange potential. The medium-range potential contains the 2ϕ-exchange potential and the contributions by the Lagrangians (9)–(12). The 2ϕ-exchange potential is model independent (still renormalization-scheme dependent) since there are no unknown constants in it, which is very essential for the medium-range interaction of the heavy pseudoscalar mesons. The interaction induced only by the 2ϕ exchange is repulsive in the channels $\bar{B}\bar{B}^{I=0}$, $DD^{I=0}$, while attractive in the other channels. Unfortunately the leading order coupling constants from the contact terms and LECs at $O(\epsilon^2)$ remain undetermined due to the lack of experimental data.

Once these LECs are extracted from lattice QCD simulation, other model approaches, or future experimental measurements, the potentials derived in this work can be used to study the possible molecular states or scattering phase shift of the two-heavy-pseudoscalar-meson system. On the other hand, the analytical chiral structures of the potentials of the heavy meson pair may be useful in the extrapolation of the heavy meson interaction from lattice QCD simulation.

ACKNOWLEDGMENTS

This project was supported by the National Natural Science Foundation of China under Grants No. 11075004, No. 11021092, and No. 11261130311 and Ministry of Science and Technology of China (No. 2009CB825200). This work is also supported in part by the DFG and the NSFC through funds provided to the sino-germen CRC 110 "Symmetries and the Emergence of Structure in QCD."

APPENDIX A: SOME FUNCTIONS USED FOR POTENTIALS

The J functions can be obtained by calculating the following integrals in D dimensions:

$$i\int\frac{d^Dl\lambda^{4-D}}{(2\pi)^D}\frac{\{1,l^\alpha,l^\alpha l^\beta,l^\alpha l^\beta l^\gamma\}}{(v\cdot l+\omega+i\varepsilon)(l^2-m^2+i\varepsilon)}\equiv\{J^a_0,v^\alpha J^a_{11},v^\alpha v^\beta J^a_{21}+g^{\alpha\beta}J^a_{22},(g\vee v)J^a_{31}+v^\alpha v^\beta v^\gamma J^a_{32}\}(m,\omega),\tag{A1}$$

$$i\int\frac{d^Dl\lambda^{4-D}}{(2\pi)^D}\frac{\{1,l^\alpha,l^\alpha l^\beta\}}{(l^2-m^2+i\varepsilon)}\equiv\{J^c_0,0,g^{\alpha\beta}J^c_{21}\}(m),\tag{A2}$$

$$\begin{aligned}&i\int\frac{d^Dl\lambda^{4-D}}{(2\pi)^D}\frac{\{1,l^\alpha,l^\alpha l^\beta,l^\alpha l^\beta l^\gamma\}}{(v\cdot l+\omega+i\varepsilon)[(+/-)v\cdot l+\delta+i\varepsilon]_s(l^2-m^2+i\varepsilon)}\\&\equiv\{J^{g/h}_0,v^\alpha J^{g/h}_{11},v^\alpha v^\beta J^{g/h}_{21}+g^{\alpha\beta}J^{g/h}_{22},(g\vee v)J^{g/h}_{31}+v^\alpha v^\beta v^\gamma J^{g/h}_{32}\}(m,\omega,\delta),\end{aligned}\tag{A3}$$

$$i\int\frac{d^Dl\lambda^{4-D}}{(2\pi)^D}\frac{\{1,l^\alpha,l^\alpha l^\beta,l^\alpha l^\beta l^\gamma\}}{(l^2-m^2+i\varepsilon)[(q+l)^2-M^2+i\varepsilon]}\equiv\{J^F_0,q^\alpha J^F_{11},q^\alpha q^\beta J^F_{21}+g^{\alpha\beta}J^F_{22},(g\vee q)J^F_{31}+q^\alpha q^\beta q^\gamma J^F_{32}\}(m,M,q),\tag{A4}$$

$$
\begin{aligned}
&i\int\frac{d^Dl\lambda^{4-D}}{(2\pi)^D}\frac{\{1,l^\alpha,l^\alpha l^\beta,l^\alpha l^\beta l^\gamma,l^\alpha l^\beta l^\gamma l^\delta\}}{(v\cdot l+\omega+i\varepsilon)(l^2-m^2+i\varepsilon)[(q+l)^2-M^2+i\varepsilon]}\\
&\equiv\{J_0^T,q^\alpha J_{11}^T+v^\alpha J_{12}^T,g^{\alpha\beta}J_{21}^T+q^\alpha q^\beta J_{22}^T+v^\alpha v^\beta J_{23}^T+(q\vee v)J_{24}^T,(g\vee q)J_{31}^T+q^\alpha q^\beta q^\gamma J_{32}^T+(q^2\vee v)J_{33}^T+(g\vee v)J_{34}^T\\
&\quad+(q\vee v^2)J_{35}^T+v^\alpha v^\beta v^\gamma J_{36}^T,(g\vee g)J_{41}^T+(g\vee q^2)J_{42}^T+q^\alpha q^\beta q^\gamma q^\delta J_{43}^T+(g\vee v^2)J_{44}^T+v^\alpha v^\beta v^\gamma v^\delta J_{45}^T+(q^3\vee v)J_{46}^T\\
&\quad+(q^2\vee v^2)J_{47}^T+(q\vee v^3)J_{48}^T+(g\vee q\vee v)J_{49}^T\}(m,M,\omega,q),
\end{aligned}
\tag{A5}
$$

$$
\begin{aligned}
&i\int\frac{d^Dl\lambda^{4-D}}{(2\pi)^D}\frac{\{1,l^\alpha,l^\alpha l^\beta,l^\alpha l^\beta l^\gamma,l^\alpha l^\beta l^\gamma l^\delta\}}{(v\cdot l+\omega+i\varepsilon)[(+/-)v\cdot l+\delta+i\varepsilon]_s(l^2-m^2+i\varepsilon)[(q+l)^2-M^2+i\varepsilon]}\\
&\equiv\{J_0^{R/B},q^\alpha J_{11}^{R/B}+v^\alpha J_{12}^{R/B},g^{\alpha\beta}J_{21}^{R/B}+q^\alpha q^\beta J_{22}^{R/B}+v^\alpha v^\beta J_{23}^{R/B}+(q\vee v)J_{24}^{R/B},(g\vee q)J_{31}^{R/B}+q^\alpha q^\beta q^\gamma J_{32}^{R/B}+(q^2\vee v)J_{33}^{R/B}\\
&\quad+(g\vee v)J_{34}^{R/B}+(q\vee v^2)J_{35}^{R/B}+v^\alpha v^\beta v^\gamma J_{36}^{R/B},(g\vee g)J_{41}^{R/B}+(g\vee q^2)J_{42}^{R/B}+q^\alpha q^\beta q^\gamma q^\delta J_{43}^{R/B}+(g\vee v^2)J_{44}^{R/B}+v^\alpha v^\beta v^\gamma v^\delta J_{45}^{R/B}\\
&\quad+(q^3\vee v)J_{46}^{R/B}+(q^2\vee v^2)J_{47}^{R/B}+(q\vee v^3)J_{48}^{R/B}+(g\vee q\vee v)J_{49}^{R/B}\}(m,M,\omega,\delta,q),
\end{aligned}
\tag{A6}
$$

where we have used the following Feynman rule for propagators of two heavy mesons in HMχPT to remove the 2PR contributions from the Feynman diagrams:

$$
\frac{1}{(v\cdot l+\omega+i\varepsilon)[(\mathrm{sgn})v\cdot l+\delta+i\varepsilon]_s}\equiv\begin{cases}\frac{1}{(v\cdot l+\omega+i\varepsilon)}\left[(-)\frac{1}{v\cdot l+\omega+i\varepsilon}-2\pi i\delta(v\cdot l+\omega)\right]_s\equiv(-)\frac{1}{(v\cdot l+\omega+i\varepsilon)^2} & \mathrm{sgn}=-,\delta=-\omega\\ \frac{1}{(v\cdot l+\omega+i\varepsilon)[(\mathrm{sgn})v\cdot l+\delta+i\varepsilon]} & \text{other}\end{cases}.
\tag{A7}
$$

The notation $X\vee Y\vee Z\vee\cdots$ represents the symmetrized tensor of $X^\alpha Y^\beta Z^\gamma\cdots$, and in detail,

$$
\begin{aligned}
q\vee v&\equiv q^\alpha v^\beta+q^\beta v^\alpha,\qquad g\vee q\equiv g^{\alpha\beta}q^\gamma+g^{\alpha\gamma}q^\beta+g^{\gamma\beta}q^\alpha,\qquad g\vee v\equiv g^{\alpha\beta}v^\gamma+g^{\alpha\gamma}v^\beta+g^{\gamma\beta}v^\alpha,\\
q^2\vee v&\equiv q^\beta q^\gamma v^\alpha+q^\alpha q^\gamma v^\beta+q^\alpha q^\beta v^\gamma,\qquad q\vee v^2\equiv q^\gamma v^\alpha v^\beta+q^\beta v^\alpha v^\gamma+q^\alpha v^\beta v^\gamma,\\
g\vee g&\equiv g^{\alpha\beta}g^{\gamma\delta}+g^{\alpha\delta}g^{\beta\gamma}+g^{\alpha\gamma}g^{\beta\delta},\qquad g\vee q^2\equiv q^\alpha q^\beta g^{\gamma\delta}+q^\alpha q^\delta g^{\beta\gamma}+q^\alpha q^\gamma g^{\beta\delta}+q^\gamma q^\delta g^{\alpha\beta}+q^\beta q^\delta g^{\alpha\gamma}+q^\beta q^\gamma g^{\alpha\delta},\\
g\vee v^2&\equiv v^\alpha v^\beta g^{\gamma\delta}+v^\alpha v^\delta g^{\beta\gamma}+v^\alpha v^\gamma g^{\beta\delta}+v^\gamma v^\delta g^{\alpha\beta}+v^\beta v^\delta g^{\alpha\gamma}+v^\beta v^\gamma g^{\alpha\delta},\\
q^3\vee v&\equiv q^\beta q^\gamma q^\delta v^\alpha+q^\alpha q^\gamma q^\delta v^\beta+q^\alpha q^\beta q^\delta v^\gamma+q^\alpha q^\beta q^\gamma v^\delta,\qquad q\vee v^3\equiv q^\delta v^\alpha v^\beta v^\gamma+q^\gamma v^\alpha v^\beta v^\delta+q^\beta v^\alpha v^\gamma v^\delta+q^\alpha v^\beta v^\gamma v^\delta,\\
q^2\vee v^2&\equiv q^\gamma q^\delta v^\alpha v^\beta+q^\beta q^\delta v^\alpha v^\gamma+q^\alpha q^\delta v^\beta v^\gamma+q^\beta q^\gamma v^\alpha v^\delta+q^\alpha q^\gamma v^\beta v^\delta+q^\alpha q^\beta v^\gamma v^\delta,\\
g\vee q\vee v&\equiv q^\beta v^\alpha g^{\gamma\delta}+q^\alpha v^\beta g^{\gamma\delta}+q^\delta v^\alpha g^{\beta\gamma}+q^\gamma v^\alpha g^{\beta\delta}+q^\alpha v^\delta g^{\beta\gamma}+q^\alpha v^\gamma g^{\beta\delta}+q^\delta v^\gamma g^{\alpha\beta}+q^\delta v^\beta g^{\alpha\gamma}+q^\gamma v^\delta g^{\alpha\beta}\\
&\quad+q^\gamma v^\beta g^{\alpha\delta}+q^\beta v^\delta g^{\alpha\gamma}+q^\beta v^\gamma g^{\alpha\delta}.
\end{aligned}
\tag{A8}
$$

APPENDIX B: ESTIMATION OF CONTRIBUTIONS FROM THE LECs AT $O(\epsilon^2)$

We will estimate the contributions of the LECs to the potentials at order $O(\epsilon^2)$, based on the data from the quenched lattice QCD study in the two-flavor case [42]. In the quenched QCD, the "quark-flow approach" or "quenched chiral perturbation theory" should be used to get the potential [43–45]. In what follows, we apply for the quark-flow approach in which one uses the ordinary chiral Lagrangians but should eliminate all diagrams containing virtual quark loops. As an estimation, we roughly consider the contributions of the tree diagrams to fit the data of the quenched lattice QCD study.

To $O(\epsilon^2)$, the potential from the tree diagrams in the three-flavor case can be written as

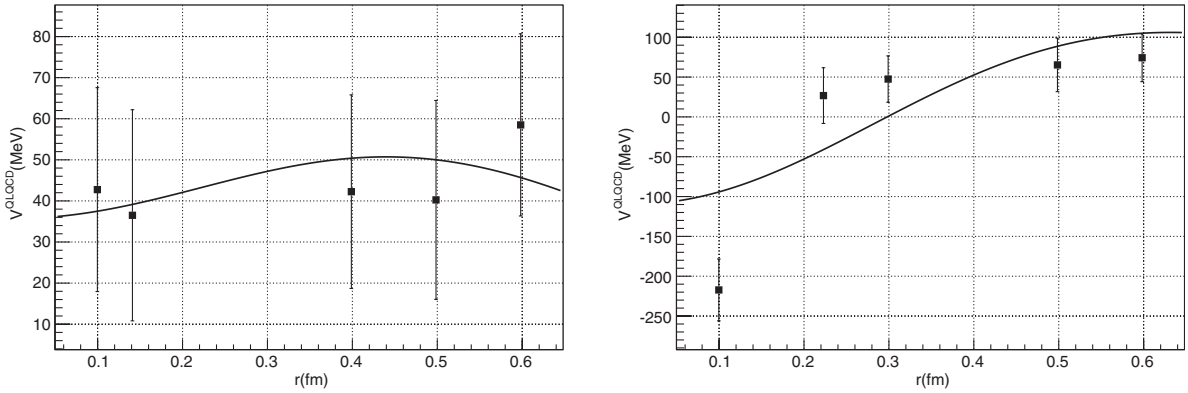

(a) $I = 0$ (b) $I = 1$

FIG. 8. Fitting the $\bar{B}\bar{B}$ potentials. The data of the quenched lattice QCD are derived from Ref. [42] where $m_\pi = 402.5 \pm 6.7$ MeV, and the error Δf is calculated with $\sqrt{\sum_i \alpha_i^2 (\Delta g_i)^2}$ if $f = \sum_i \alpha_i g_i$. The curve is obtained using Eqs. (B2) and (B3) with parameters Eq. (B5).

$$V_{ch}^{\rm tree}(\vec{q}^2) = \frac{\alpha^{ch}}{\Lambda_0^2} + \frac{\beta_1^{ch}}{\Lambda_0^4} m_\pi^2 + \frac{\beta_2^{ch}}{\Lambda_0^4} m_K^2 + \frac{\beta_3^{ch}}{\Lambda_0^4} m_\eta^2 + \frac{\gamma^{ch}}{\Lambda_0^4} \vec{q}^2, \quad \Lambda_0 = 1 \text{ GeV}, \tag{B1}$$

where α^{ch} can be obtained by Eq. (14), and β_i^{ch} and γ^{ch} are the linear combinations of LECs at $O(\epsilon^2)$. In quenched QCD, the potential in the two-flavor case can be estimated as follows:

$$V_{\bar{B}\bar{B}^I}^{\rm QQCD}(\vec{q}^2) = \frac{a^I}{\Lambda_0^2} + \frac{b^I}{\Lambda_0^4} m_\pi^2 + \frac{c^I}{\Lambda_0^4} \vec{q}^2, \qquad \Lambda_0 = 1 \text{ GeV}, \tag{B2}$$

where a^I, b^I, and c^I are similar to α^{ch}, β_i^{ch}, and γ^{ch} in the three-flavor case.

From Eq. (14) one obtains $a^0 = 0$. Introducing Gaussian form factor $\exp(-\vec{q}^2/\Lambda_G^2)$, we perform the Fourier transformation to get the potential in the coordinate space,

$$V(\vec{r}) = \frac{1}{(2\pi)^3} \int d^3\vec{q} \left[\frac{1}{4} V(\vec{q}^2) \right] e^{-\vec{q}^2/\Lambda_G^2} e^{-i\vec{q}\cdot\vec{r}}. \tag{B3}$$

The specific expression of the potential is

$$V_{\bar{B}\bar{B}^I}^{\rm QQCD}(r) = \frac{1}{4} \frac{\Lambda_G^3 \exp(-\frac{1}{4}\Lambda_G^2 r^2)}{32\pi^{3/2}} \left[4\left(\frac{a^I}{\Lambda_0^2} + \frac{b^I}{\Lambda_0^4} m_\pi^2 \right) + \frac{c^I}{\Lambda_0^4} \Lambda_G^2 (6 - \Lambda_G^2 r^2) \right]. \tag{B4}$$

By fitting the results of the quenched lattice QCD [42], we obtain with $\chi^2_{\rm d.o.f} = 3.7$

$$a^0 = 0, \qquad b^0 = 94 \pm 38, \qquad c^0 = -16 \pm 9,$$
$$a^1 + 0.16 b^1 = 42 \pm 8, \qquad c^1 = -69 \pm 13,$$
$$\Lambda_G = 708 \pm (2 \times 10^{-9}) \text{ MeV}. \tag{B5}$$

We show the lattice data and the fitted curve in Fig. 8. However, we cannot determine a^1 and b^1, respectively, since the results of the lattice study are given with only one set of $m_\pi = 402.5 \pm 6.7$ MeV.

With these values of a^I, b^I, and c^I from the lattice simulation, we can discuss the potential at the physical pion mass now. The potential $V_{\bar{B}\bar{B}^0}$ contains three parts up to $O(\epsilon^2)$: $V_{\bar{B}\bar{B}^0}^{(2,\rm LEC)}$ from LECs at $O(\epsilon^2)$, the 2π-exchange contribution $V_{\bar{B}\bar{B}^0}^{(2,2\pi)}$, and loop corrections to the contact terms $V_{\bar{B}\bar{B}^0}^{(2,\rm cont)}$. Presently we cannot determine the third term since there is only one set of data with $m_\pi = 402.5 \pm 6.7$ MeV. We obtain the first term with the value of $b^0 = 94$ and $c^0 = -16$, and the second term by turning off the propagation of kaon and eta. As $|\vec{q}|$ goes from 0 to 300 MeV, $V_{\bar{B}\bar{B}^0}^{(2,\rm LEC)}$ changes from 1.8 GeV^{-2} to 0.4 GeV^{-2}, and $V_{\bar{B}\bar{B}^0}^{(2,2\pi)}$ changes from -0.88 GeV^{-2} to -6.6 GeV^{-2}. Thus the potential induced by the LECs is repulsive, whereas the 2π-exchange potential is attractive. The potential induced by the first and the second terms is repulsive but very weak at extremely small momentum in the case without the contributions of kaon or eta, and it becomes attractive when $|\vec{q}|$ is hundreds of MeV. If b^0 and c^0 take values in the interval $(-10, 10)$, $V_{\bar{B}\bar{B}^0}^{(2,\rm LEC)}$ is 0.2 GeV^{-2} uppermost, and it is smaller than $|V_{\bar{B}\bar{B}^0}^{(2,2\pi)}|$.

[1] S. K. Choi *et al.* (Belle Collaboration), Phys. Rev. Lett. **91**, 262001 (2003).
[2] K. Abe *et al.* (Belle Collaboration), Phys. Rev. Lett. **98**, 082001 (2007).
[3] P. Pakhlov *et al.* (Belle Collaboration), Phys. Rev. Lett. **100**, 202001 (2008).
[4] I. Adachi *et al.* (Belle Collaboration), arXiv:1105.4583.
[5] Y.-B. Yang, Y. Chen, L.-C. Gui, C. Liu, Y.-B. Liu, Z. Liu, J.-P. Ma, and J.-B. Zhang, Phys. Rev. D **87**, 014501 (2013).
[6] W. Chen and S.-L. Zhu, Phys. Rev. D **83**, 034010 (2011).
[7] Y.-R. Liu and Z.-Y. Zhang, Phys. Rev. C **79**, 035206 (2009).
[8] M. T. AlFiky, F. Gabbiani, and A. A. Petrov, Phys. Lett. B **640**, 238 (2006).
[9] C. E. Thomas and F. E. Close, Phys. Rev. D **78**, 034007 (2008).
[10] X. Liu, Z.-G. Luo, Y.-R. Liu, and S.-L. Zhu, Eur. Phys. J. C **61**, 411 (2009).
[11] Z.-F. Sun, J. He, X. Liu, Z.-G. Luo, and S.-L. Zhu, Phys. Rev. D **84**, 054002 (2011).
[12] S. Ohkoda, Y. Yamaguchi, S. Yasui, K. Sudoh, and A. Hosaka, Phys. Rev. D **86**, 014004 (2012).
[13] P. Cho, Nucl. Phys. **B396**, 183 (1993).
[14] V. Bernard, N. Kaiser, and U. Meissner, Nucl. Phys. **A615**, 483 (1997).
[15] T. R. Hemmert, B. R. Holstein, and J. Kambor, J. Phys. G **24**, 1831 (1998).
[16] Z.-W. Liu and S.-L. Zhu, Phys. Rev. D **86**, 034009 (2012).
[17] L. Geng, J. Camalich, L. Alvarez-Ruso, and M. Vacas, Phys. Rev. Lett. **101**, 222002 (2008).
[18] S. Weinberg, Phys. Lett. B **251**, 288 (1990).
[19] S. Weinberg, Nucl. Phys. **B363**, 3 (1991).
[20] V. Bernard, N. Kaiser, and U.-G. Meißner, Int. J. Mod. Phys. E **04**, 193 (1995).
[21] C. Ordóñez, L. Ray, and U. van Kolck, Phys. Rev. C **53**, 2086 (1996).
[22] N. Kaiser, R. Brockmann, and W. Weise, Nucl. Phys. **A625**, 758 (1997).
[23] N. Kaiser, S. Gerstendörfer, and W. Weise, Nucl. Phys. **A637**, 395 (1998).
[24] E. Epelbaoum, W. Glökle, and U.-G. Meißner, Nucl. Phys. **A637**, 107 (1998).
[25] E. Epelbaoum, W. Glökle, and U.-G. Meißner, Nucl. Phys. **A671**, 295 (2000).
[26] R. Machleidt and D. R. Entem, Phys. Rep. **503**, 1 (2011).
[27] N. Kaiser, Phys. Rev. C **64**, 057001 (2001).
[28] E. Epelbaum, U. Meißner, and W. Glöckle, Nucl. Phys. **A714**, 535 (2003).
[29] E. Epelbaum, W. Gloeckle, and U. Meißner, Nucl. Phys. **A747**, 362 (2005).
[30] S.-L. Zhu, C. M. Maekawa, B. R. Holstein, M. J. Ramsey-Musolf, and U. van Kolck, Nucl. Phys. **A748**, 435 (2005).
[31] C. Hidalgo-Duque, J. Nieves, and M. Valderrama, Phys. Rev. D **87**, 076006 (2013).
[32] P. H. Timmers, W. A. van der Sanden, and J. J. de Swart, Phys. Rev. D **29**, 1928 (1984).
[33] T. Hippchen, J. Haidenbauer, K. Holinde, and V. Mull, Phys. Rev. C **44**, 1323 (1991).
[34] M. Lüscher and U. Wolff, Nucl. Phys. **B339**, 222 (1990).
[35] R. Gupta, A. Patel, and S. R. Sharpe, Phys. Rev. D **48**, 388 (1993).
[36] G. Ming *et al.*, Chin. Phys. C **34**, 1372 (2010).
[37] M. F. M. Lutz, D. Samart, and A. Semke, Phys. Rev. D **84**, 096015 (2011).
[38] J. Beringer *et al.* (Particle Data Group), Phys. Rev. D **86**, 010001 (2012).
[39] Z.-W. Liu, Y.-R. Liu, X. Liu, and S.-L. Zhu, Phys. Rev. D **84**, 034002 (2011).
[40] H. Ohki, H. Matsufuru, and T. Onogi, Phys. Rev. D **77**, 094509 (2008).
[41] W. Detmold, C. J. D. Lin, and S. Meinel, Phys. Rev. D **85**, 114508 (2012).
[42] W. Detmold, K. Orginos, and M. J. Savage (NPLQCD Collaboration), Phys. Rev. D **76**, 114503 (2007).
[43] G. W. Kilcup, S. R. Sharpe, R. Gupta, and A. Patel, Phys. Rev. Lett. **64**, 25 (1990).
[44] C. W. Bernard and M. F. L. Golterman, Phys. Rev. D **46**, 853 (1992).
[45] J. N. Labrenz and S. R. Sharpe, Phys. Rev. D **54**, 4595 (1996).